Chapter 3

DATA AQUISITION AND PROCESSING

As discussed in the previous Chapter, first an isothermal pressure experiment was run, followed by an isobar temperature program. The pressure was built up in steps of 10 MPa up to 100 MPa, and then in steps of 20 MPa up to 200 MPa. Between 200 MPa and 1 GPa the steps were 50 MPa. Because the pressure in the vessel increases with temperature, the pressure was slowly reduced from 1 GPa to 900 MPa, before the temperature program was started. The temperature was arised in increments of 50 K using a heating rate of 2 °C/min. At each pressure and temperature step the traveltimes of elastic waves were recorded. Time was given to the sample to adjust to the *PT* conditions prior to the measurements: 45 min and 30 min passed in pressure and temperature experiments, respectively. In some pressure runs, a long-lasting system equilibration of several days was favoured. Sufficiently constant pressure conditions were obtained by a continuous pressure regulation. The temperature regime was operated with a Eurotherm controller in combination with a DC-power supply to reduce electrical noise.

3.1 Methods of Traveltime Determination

The elastic wave velocity of a system is highly sensitive to variations in pressure and temperature. To quantify these dependencies, the traveltimes of ultrasonic waves were measured under variable pressure and temperature conditions. The assembly consists of a sample and two buffer rods. Due to their different chemical composition and microstructure, sample and buffers react differently to the experimental conditions. To deduce the traveltime through the sample at each pressure and temperature step, a differential measuring procedure of wave traveltimes was used, combining the *pulse transmission method* [Birch, 1960] with the *pulse echo technique* [Lazarus, 1949; Anderson & Liebermann, 1968]. For both methods it is assumed that the wave takes the shortest path through the assembly, which corresponds to the length of the system. In case of the *pulse transmission mode* an ultrasonic wave passes through the entire set-up. The one-way arrival-time t_D consists of the traveltime through the buffer rods (t_{b_1}, t_{b_2}) and that of the rock sample (t_r) (Fig. 3.1). Assuming symmetry of the assembly, t_{b_1} equals t_{b_2}, then t_D can be

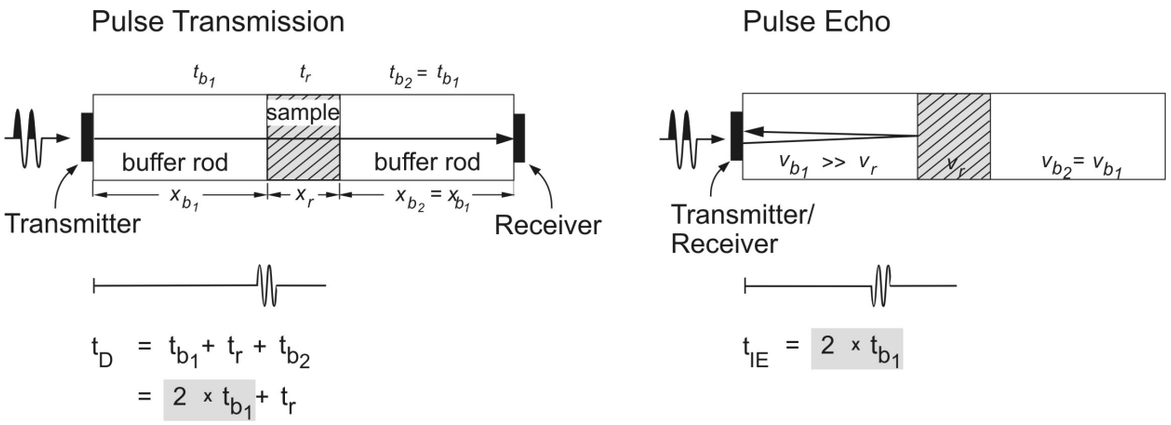

Figure 3.1: *Schematic illustration of the determination of traveltimes by the pulse-transmission and the pulse-echo techniques. In the pulse-echo mode the impedance contrast between buffer rod and rock sample ($v_b > v_r$) evokes a phase shift of the reflected wave by 180°, which has to be taken into account for the analysis of traveltimes.*

expressed by

$$t_D = 2 \cdot t_b + t_r. \tag{3.1}$$

With increasing pressure and temperature, traveltimes change in the buffer rods, which cannot be controlled using the pulse transmission method alone. To enhance the resolution and to account for possible variations under changing *PT* conditions additionally the *pulse echo method* was used and thus the information of phases, which are reflected at the interface between buffer rod and sample (Fig. 3.1). The traveltime of the first echo corresponds to twice the length of the buffer rod:

$$t_{IE} = 2 \cdot t_b. \tag{3.2}$$

t_D and t_{IE} were corrected for the dead time of the recording device (transducer, function generator, oscilloscope), which was determined at ambient conditions. Combining Eqs. 3.1 and 3.2, the velocity is deduced from the traveltime through the sample and the sample length *l*,

$$\mathrm{v}_r = \frac{l}{t_D - t_{IE}}. \tag{3.3}$$

Changes in the sample length due to increasing pressure cannot be measured directly during the experiment. Therefore, a correction is made from determined velocities v_p, v_s and the rock density ρ_0 at 1 bar, using the approximation after Gebrande [1982]:

$$\frac{l(P)}{l_0} = \left[1 + \frac{1}{\rho_0} \int_0^P \frac{1}{v_p^2 - \frac{4}{3} v_s^2} dP \right]^{-\frac{1}{3}}, \tag{3.4}$$

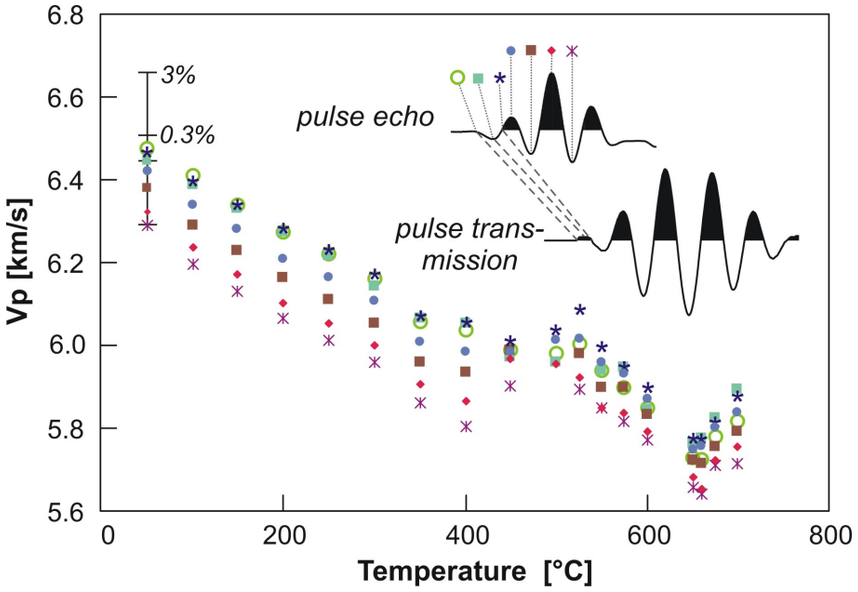

Figure 3.2: *The velocities are calculated from traveltime differences of constant phases of the pulse echo and pulse transmission signals. Note, that the pulse echo signal is inverted by* 180°*, due to the impedance contrast between buffer rod and sample. When the signal onset was diffuse, the first maximum–minimum pair was picked. The figure shows, that this procedure sligthly increases the error by* $\sim$ 0.3 % *on the elastic wave velocities. The error may increase to 1 % for picking the second minimum–maximum and to* $\sim$ 3 % *for the third minimum–maximum pair.*

where l_0 and *l(P)* are the sample length at 1 bar and elevated pressure, respectively, and *dP* is the pressure increment. The error in velocity determination increases considerably, when a later phase than the signal onset (*"onset"*-velocity) is picked. For the first motion of wave (in detail: signal onset, the first maximum or second zero crossing) the error in phase velocity is about 0.3 %. However, velocities deduced from later phases deviate from *"onset"*-velocity by up to 3 %.

3.2 The Recording Device

In the experimental arrangement P and S wave transducers with an Eigenfrequenz of 1 or 2 MHz, respectively, are stimulated alternately. To initiate an elastic wave, either a sinusoidal wavelet of a defined frequency and number of cycles was created by a programmable function generator (model AWG-Tektronix; Fig. 3.3 a) or a high-voltage pulse was sent from the Panametrix pulser/ amplifier system (Fig. 3.3 b). Both, function generator and oscilloscope are triggered by the Panametrix pulser/ amplifier with a repeating rate of 100 Hz. The initiating signals are guided through shielded cables (BNC) to the electrical lead-throughs, and inside the pressure vessel through further shielded cables to the ultrasonic transducers. The lead-through isolation was adjusted to the 50 Ω-BNC cables to reduce signal echos from the BNC cable – lead-through contact. For an easier handling, the transducers are connected to a

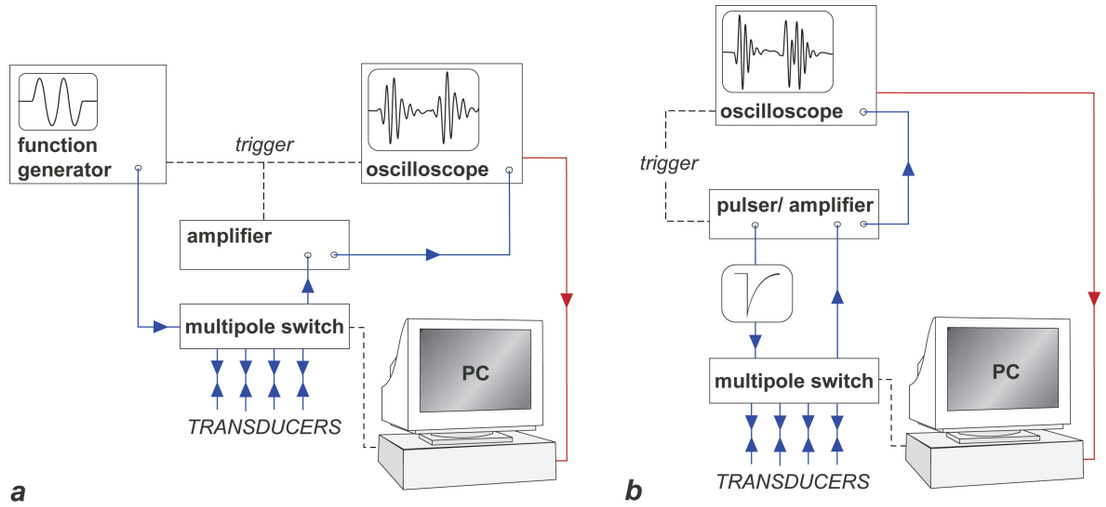

Figure 3.3: *Schematic diagrams for different types of signal generation. (a) Sinusoidal input signals were produced with a programmable function generator (Tektronix AWG 2021). (b) Alternatively, transducers were stimulated by a sharp negative impulse of a high voltage ($>$ 100 V), directly generated with the combined pulser/ amplifier system (Panametrix).*

multipole switch box. The switching between P and S wave and the transmission and pulse – echo modi, respectively, is controlled via a LabView program using a PC. Subsequently, the received signals are low and high pass filtered with 3 and 0.3 MHz, respectively and boosted in the pulser/ amplifier system and transmitted to the digital oscilloscope. There, the signals from 1024 runs are stacked, digitized at a sample rate of 0.004 μs, and read out in ASCII-format. The digital data are transferred to the PC via IEEE interface.

3.3 Processing Methodology

Seismograms recorded in transmission as well as in pulse echo mode are a superposition of various phases, consequently their interpretation becomes very complex (Fig. 3.4). Besides the direct waves, several sidewall reflections are induced due to the limited lateral extension of the assembly. Moreover, additional phases appear in the seismograms, that may be interpreted as P to S reflections or even multiple reflections (PSP). This is indicated by measurements, where a wave is transmitted by a P-transducer and recorded with a P- and S-receiver, respectively (Fig. 3.5). In this case the second ($PS^?$) and third ($S^?$) phase show a high amplitude, when recorded with the S-receiver. Equivalent observations were made with an S-transmitter/ P-transducer pair.

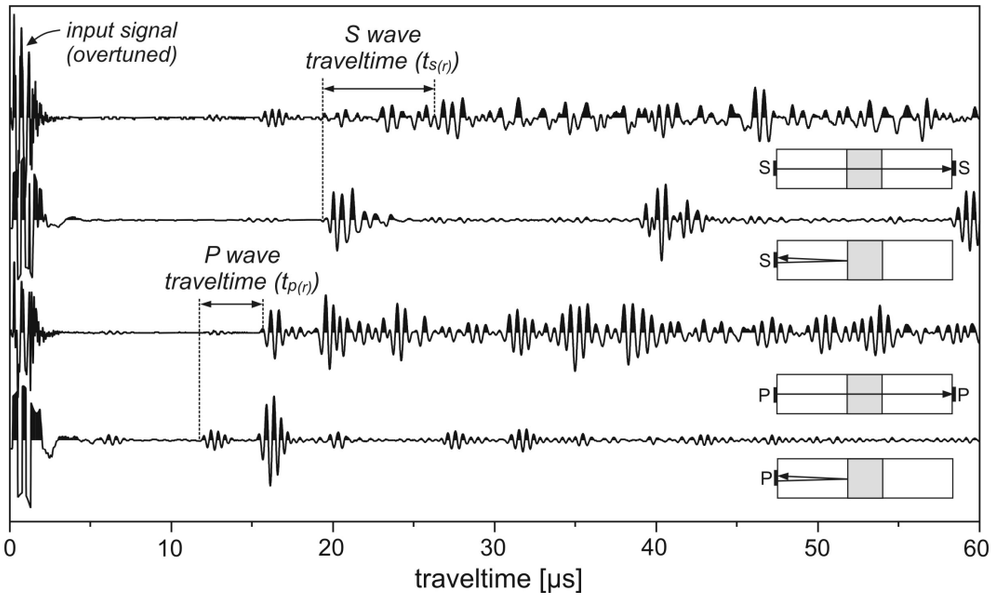

Figure 3.4: *Traveltime traces at ambient PT conditons (excitation frequency: 2 MHz). The dotted lines mark the onset of P-transmission, P-echo, S-transmission, and S-echo signals, respectively (from bottom to top).* $t_{p_{(r)}}$ *= P wave traveltime through sample;* $t_{s_{(r)}}$ *= S wave traveltime through sample.*

The operation of a shear transducer always generates in addition to the S wave a secondary low energy P wave. In the pulse echo mode the energy difference between the secondary P wave and the S waves possibly is too large to record pronounced sidewall reflections (Fig. 3.4). However, in transmission mode P to S reflections probably occur. A strong reflected phase appears at around 24 μs and thus immediately before the direct S wave ($\sim$ 26 μs) of the amphibolite (upper line Fig. 3.4). Unfortunately, increasing the pressure lowers the traveltime of the direct wave much more than that of the reflected one. Hence both phases superimpose, and the signal onset of the S wave, especially of the amphibolite samples, may be concealed.

Except in the *S – pulse echo* trace (upper trace in Fig. 3.4), multiples of the direct phase are superimposed by sidewall reflections and cannot be used for data analysis. For this reason it is essential, that the direct wave is minimally affected by noise. Especially in pulse echo mode the noise level is high due to ringing, since signal transmission and recording are carried out with the same transducer. To reduce the overlap of the ringing of the transducer with the signals, the tests of an appropriate damping material, mentioned above, were extremely important.

Generally, the superposition of phases could be reduced by shortening of the input signal and the increase of excitation frequency. However, when activating the transducers with a short needle pulse, the recorded signals are distorted to some degree. The best response from the used transducers resulted from the activation with an incident sinusoidal wavelet of two cycles. Moreover, due to damping of elastic wave energy in the sample, no excitation frequency higher than 2 MHz was used.

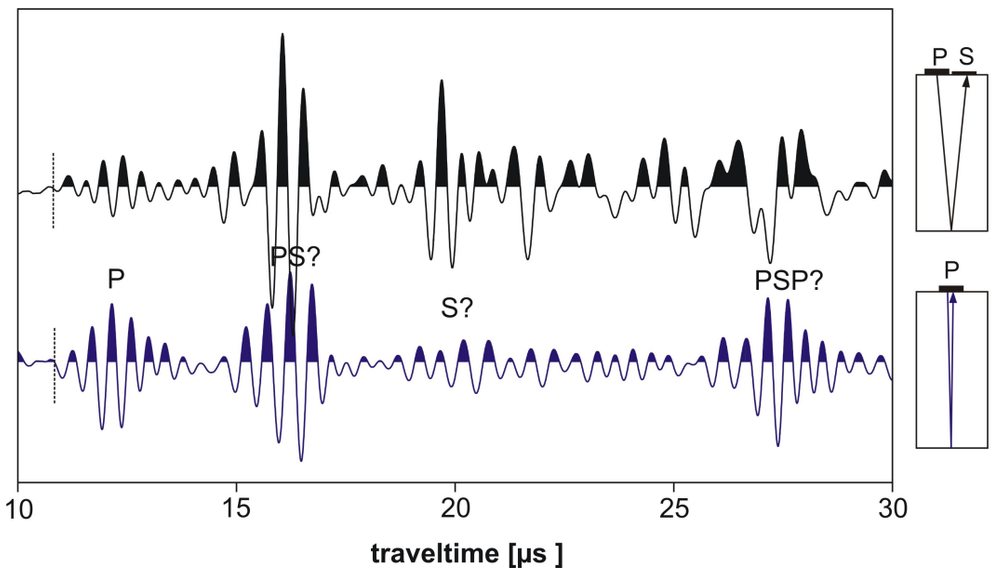

Figure 3.5: *Pulse echo signals of a P wave, recorded with a P wave transducer (lower trace) and by a S wave transducer (upper trace), respectively. Note that the phases arriving after the direct P wave are characterised by high amplitudes when recorded with a S wave transducer. Dotted lines mark the onset of the P wave.*

The data processing was done with *Seismic Unix* (SU), version 3.7, an open-source seismic package, developed at the Center of Wave Phenomena at Colorado School of Mines [Stockwell & Cohen, 2002]. It is focused on application in reflection-seismic processing. The original ASCII data were converted to binary format, and after adding header information, read into SU. Some preprocessing steps, such as time-windowing, removal of constant trace offset and trace balancing were applied. If necessary, data were zero-phase bandpass filtered to enhance the signal to noise ratio. When possible, the arrival times of the direct waves were picked manually, to guarantee a most accurate picking of the signal onset. The readings are subjected to a certain error due to noise (e.g. transducer ringing or crosstalking of high frequency signals in the plug of the autoclave) and the waveform of the signals, which generally are indistinct. Where the first onset could not be picked, the first maximum or second zero crossing was picked. From this procedure an error of 0.3 % on calculated elastic wave velocities arises (Fig. 3.2).

3.3.1 Cross-correlation

To better detect weak signals embedded in noise, a cross-correlation function was applied, which exploits the similarity between source wavelet and the transmitted/ reflected direct phase and thus enhances the signal to noise ratio significantly (Fig. 3.6). Given two digital waveforms, x_i and y_i of finite length N, the cross-correlation function is

$$\phi_{xy}(\tau) = \sum_{i=1}^{N-\tau} x_i \, y_{(i+\tau)}, \tag{3.5}$$

where τ is the lag. For each value of τ the two waveforms are cross-multiplied. The summation of all products is the value of the cross-correlation function at lag τ. Cross-correlation of a waveform, which contains a reference signal concealed in noise, with the reference signal will produce a peak amplitude for the time value, at which the signals are in phase.

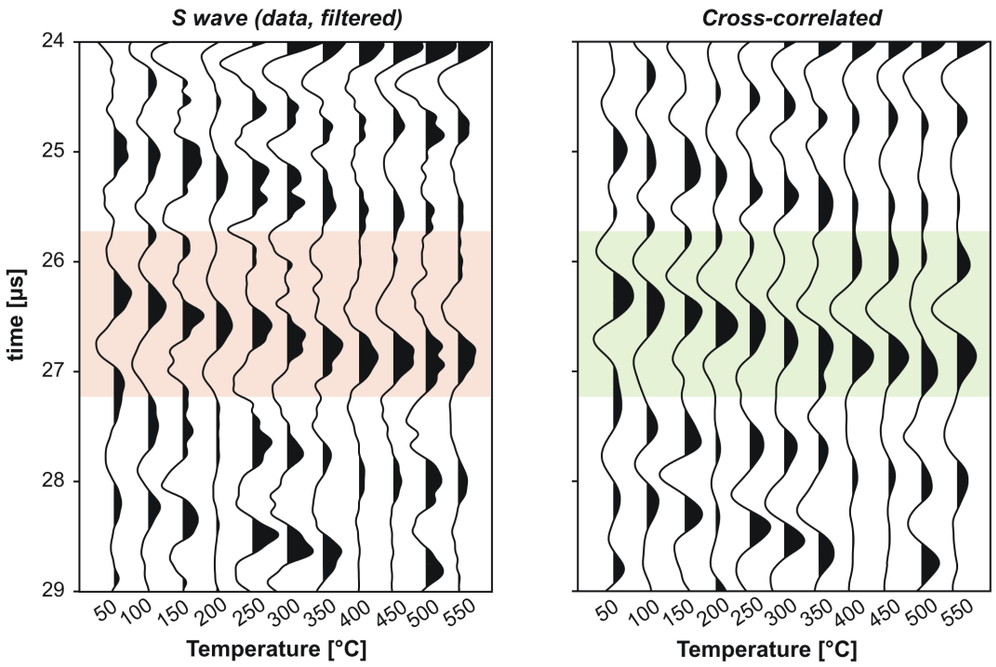

Figure 3.6: *The resolution of S waves (red shaded), measured with the pulse transmission technique, is weak, as the signals are superimposed by sidewall reflections. On the right, the result of cross-correlation is shown. The reference signal corresponds to the incident signal (one-cycle sinus of 2 MHz).*

3.3.2 Enveloping

Occasionally, the picking of signal onset-times or the analysis of cross-correlated signals was difficult or not successful. Therefore, the 'enveloping' technique was applied as an alternative tool to pick traveltimes. The maximum of the envelope of a waveform may be, in occasions, more robust to pick.
The theory of enveloping or, more general, complex trace analysis was developed in electrical engineering [Gabor, 1946; Cramer & Leadbetter, 1967]. Applications to seismic signal analysis were given, for example, by Taner et al. [1979] and references therein and by Engelhard [1996]. In the complex trace analysis the seismic trace f(t) with phase θ

$$f(t) = A(t)\ cos\theta(t) \tag{3.6}$$

and the quadrature seismic trace $f^*(t)$

$$f^*(t) = A(t)\ sin\theta(t) \tag{3.7}$$

are defined as the real and imaginary part, respectively, of a complex trace

$$F(t) = f(t) + i\, f^*(t) = A(t)\ e^{i\theta(t)}. \tag{3.8}$$

The quadrature trace is the Hilbert transform of the seismic trace. The amplitude A of the complex trace is called "reflection strength" and displays the so-called envelope of the real trace:

$$A(t) = \sqrt{[f^2(t) + f^{*2}(t)]} = |F(t)|. \tag{3.9}$$

A discussion of the method is given in more detail by Taner et al. [1979].

Generally, 2 MHz signals are more suitable for applying the 'enveloping' as the single phases are separated more clearly than in the 1 MHz recordings. Figs. 3.7 and 3.8 show the raw data of P wave traveltime traces and their corresponding envelopes for an excitation frequency of 2 MHz. The maximum amplitude of the envelope reflects the group velocity of a wave and its position is highly dependent on the signal shape. When the signal shape is not affected by changing PT conditions, the PT dependencies of velocities derived from phase and group traveltimes are identical. In Fig. 3.9 2 MHz-traveltime traces and their corresponding envelopes are compared in dependence of pressure and temperature, respectively. Furthermore, a distinction is made between seismograms, recorded in pulse echo and pulse transmission mode. The shape of 2 MHz-pulse echo signals seem to be rather unaffected by changing physical conditions, and phase and group run nearly parallel within $\pm 0.05\ \mu$s over the entire pressure and temperature range. A minor variation in signal form can be related to an overmodulation due to tuning effects of the

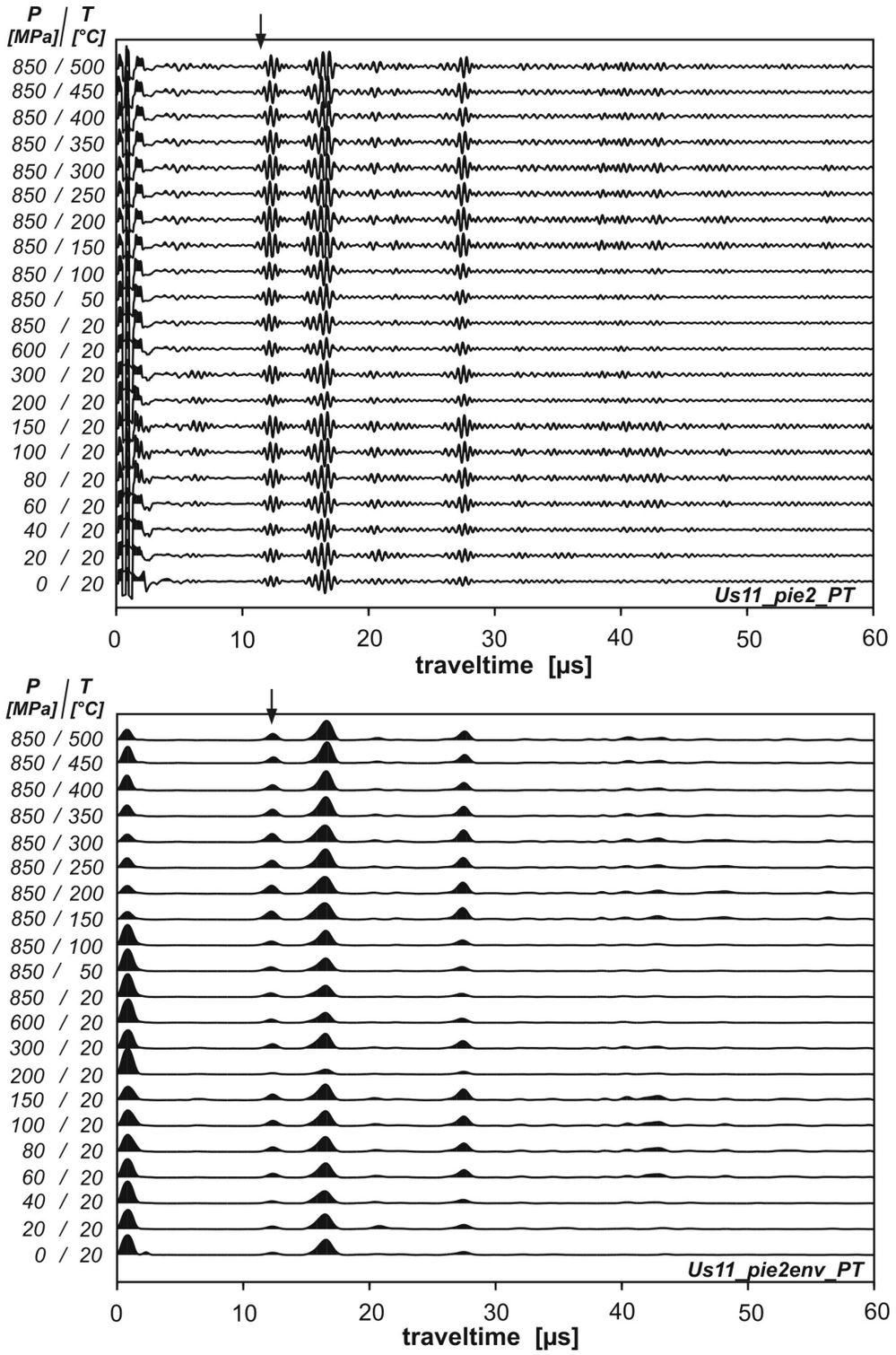

Figure 3.7: *Raw data of P wave traveltimes traces in dependence of pressure and temperature, recorded in pulse echo mode (upper diagram) and their corresponding envelopes (bottom). The excitation frequency is 2 MHz. The envelope is presented here as A^2 to sharpen the signal. The arrows mark the onset of the pulse echo signals and its maxima, respectively. The strong signal at ~ 15 µs is a sidewall reflection.*

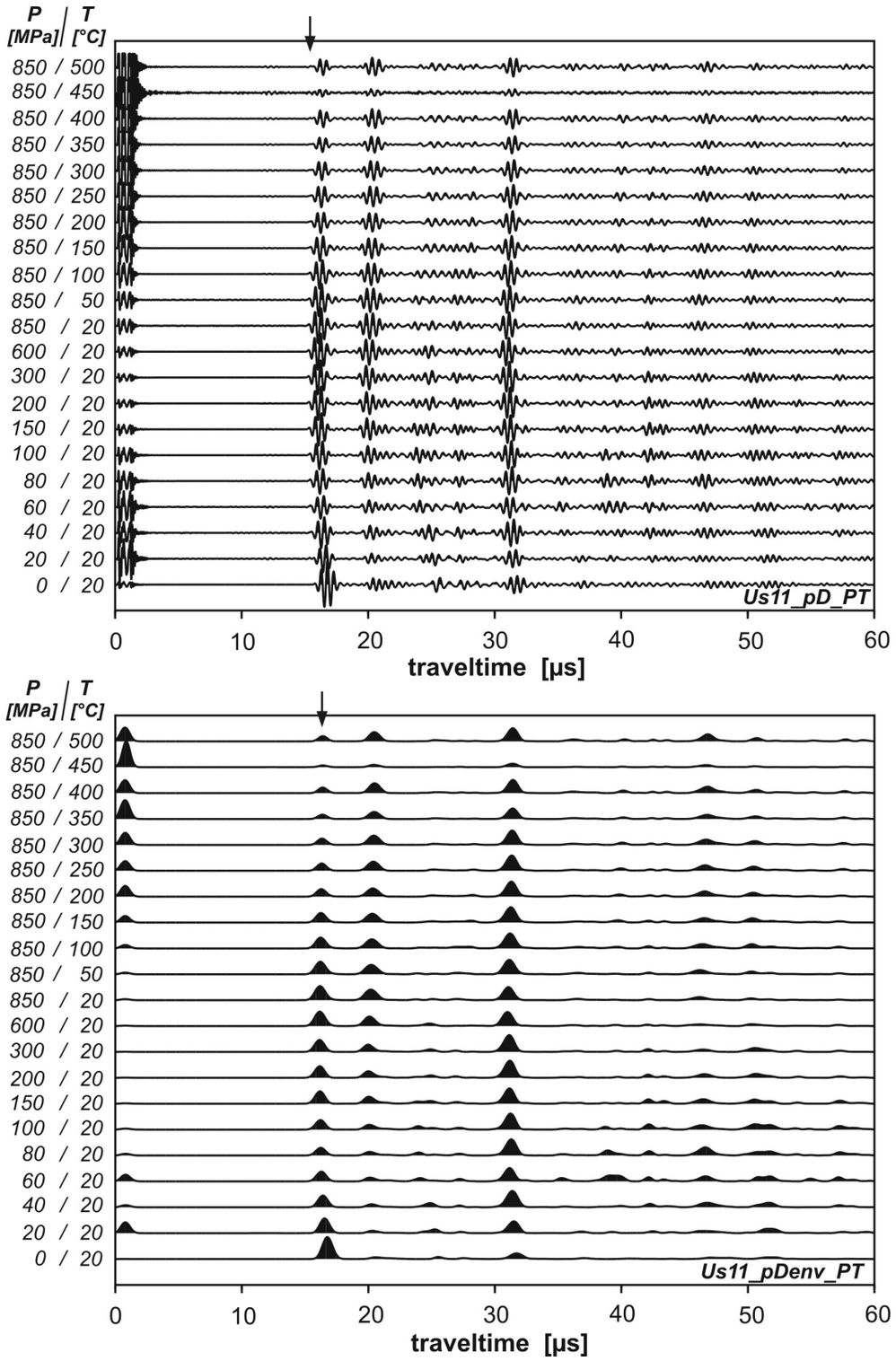

Figure 3.8: *P wave traveltimes traces in dependence of pressure and temperature, recorded in pulse transmission (top) and their corresponding envelopes (bottom). The excitation frequency is 2 MHz. The envelope is presented as A^2 to sharpen the signal.*

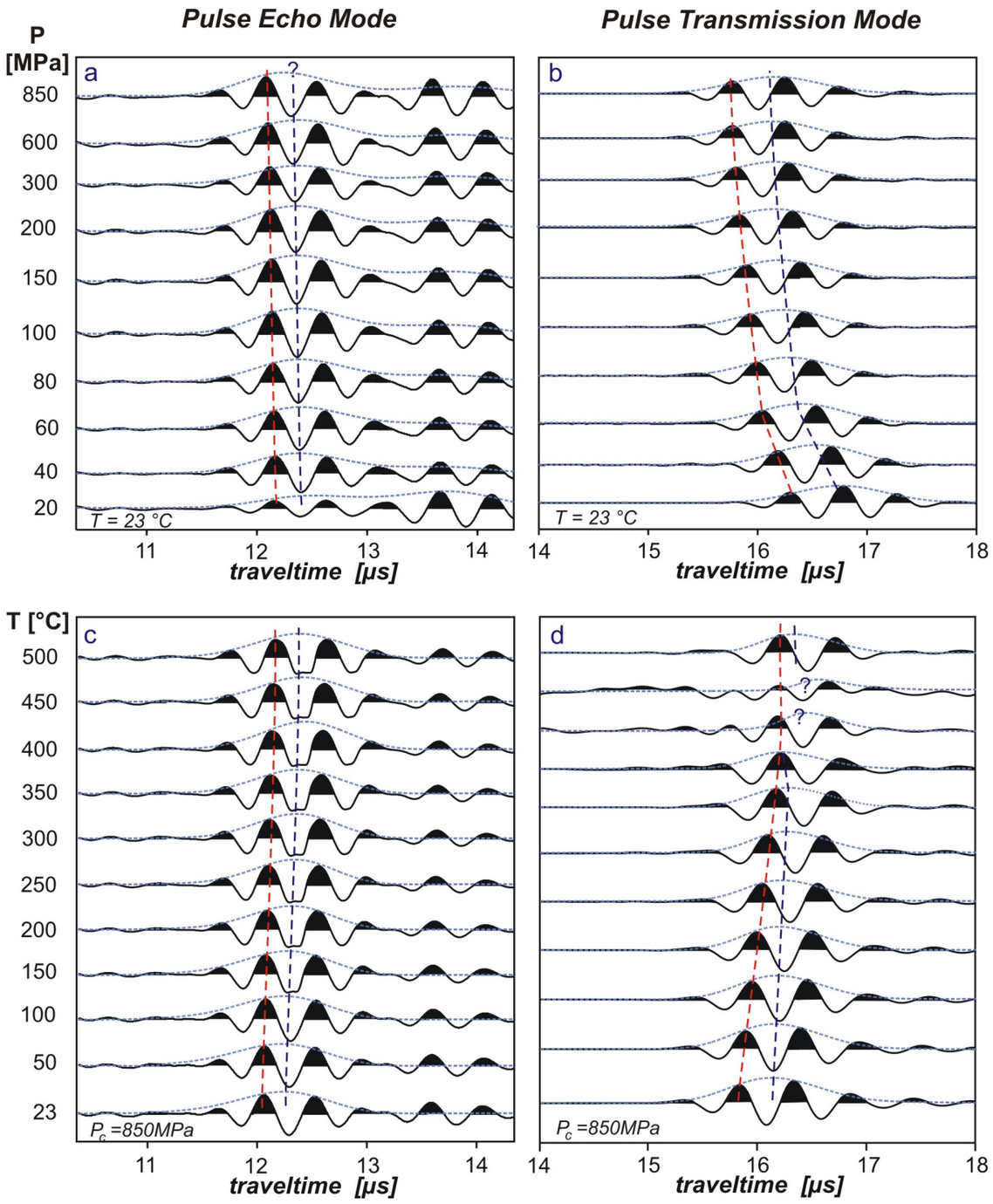

Figure 3.9: *P wave traveltime traces (black solid lines) and their corresponding envelopes (blue dotted) in dependence of pressure (a and b) and temperature (c and d). The seismograms are recorded with pulse echo (left) and pulse transmission technique (right), respectively. Red dashed lines refer to a point of constant phase velocity, the blue dashed ones to the maximum amplitude of the envelope. Note the general concordance of both velocities in (a), (b), and (c). It can be concluded, that the buffer rods are no dispersive media and the sample behave non-dispersive with increasing pressure, too. Minor changes in the pulse echo signal form for increasing temperatures is given by an overmodulation of the signal due to overtuning by the amplifier. (d) With increasing temperature the phase velocity and group velocity of pulse transmission signals converge. Note, that the change of waveform here is displayed by a reduction of the signal coda. - Envelopes are presented here as A^2. (input signal: 2 MHz, 2 wavelet)*

amplifier. In pulse transmission the waveforms remain also stable, as the pressure is raised. In contrast, the coda of the 2 MHz-signals is significantly reduced with increasing temperature, which consequently results in a convergence of phase velocity and group velocity of the transmission signals.
For 1 MHz transmission signals the comparison of the maximum of the envelope and a point of constant phase of the corresponding seismic trace reveal a concordance of the traveltimes of the phase and the group approximately over the whole pressure and temperature range.

In summary, for seismic traces, recorded at increasing pressure, the enveloping procedure offers an enhancement of precision, as the peak of the envelope is easier to pick than the signal onset. For increasing temperatures, however, the analysis of the envelopes to facilitate picking is not valid at least for 2 MHz signals, as the energy of the signal spreads with a different velocity than that of the phase.

3.4 Error Estimation

As discussed above, the traveltime determinations are – depending on signal strength – generally better than 0.02 μs, which corresponds to an uncertainty of 1 % (2σ) in the traveltime through the sample. The sample length at ambient pressure is known better than 0.01 mm or 0.04 %. The intrinsic compressibility of the rocks is approximated using Eq. 3.4 and leads to uncertainties in the overall sample length for any pressure step of less than 0.2 %. The same holds true for thermal expansion if expansion values for the minerals are taken into account; the resultant error is $\leq$ 0.1 %. Moreover, the variation in sample length due to microstructural changes is not well known. As the porosity is $<$ 2 vol% (Tab. 4.1), and all experimental observations suggest that this is the maximum porosity during the experiment, a maximum length variation due to microstructural changes is $\leq$ 0.6 %; this uncertainty is corrected by the approximation in Eq. 3.4 [Gebrande, 1982]. This leads to an overall uncertainty of velocity determination of $\sim$ 1.3 % (2σ) if a normal distribution of errors is assumed.
It is assumed that the relative velocitiy and corresponding characteristics, such as the slope of the velocity–pressure relations and the velocity–temperature relations were determined more precisely, as systematic errors will cancel out.